

Photonic Dirac cone and topological transition in a moving dielectric slab

Xinyang Pan(潘昕阳), Haitao Li(李海涛), Weijie Dong(董为杰), Xiaoxi Zhou(周萧溪), Gang Wang(王钢), and Bo Hou(侯波)

Citation: Chin. Phys. B, 2023, 32 (**10**): 107802. DOI: 10.1088/1674-1056/ace1d7
Journal homepage: http://cpb.iphy.ac.cn; http://iopscience.iop.org/cpb

What follows is a list of articles you may be interested in

Elemental composition x-ray fluorescence analysis with a TES-based high-resolution x-ray spectrometer

Bingjun Wu(吴秉骏), Jingkai Xia(夏经铠), Shuo Zhang(张硕), Qiang Fu(傅强), Hui Zhang(章辉),Xiaoming Xie(谢晓明), and Zhi Liu(刘志)
Chin. Phys. B, 2023, 32 (**9**): 097801. DOI: 10.1088/1674-1056/acd926

Magneto-optical Kerr and Faraday effects in bilayer antiferromagnetic insulators

Wan-Qing Zhu(朱婉情) and Wen-Yu Shan(单文语)
Chin. Phys. B, 2023, 32 (**8**): 087802. DOI: 10.1088/1674-1056/acd68a

An ultrafast spectroscopy system for studying dynamic properties of superconductors under high pressure and low temperature conditions

Jian Zhu(朱健), Ye-Xi Li(李叶西), Deng-Man Feng(冯登满), De-Peng Su(苏德鹏), Dong-Niu Fan(范东牛),Song Yang(杨松), Chen-Xiao Zhao(赵辰晓), Gao-Yang Zhao(赵高扬), Liang Li(李亮),Fang-Fei Li(李芳菲), Ying-Hui Wang(王英惠), and Qiang Zhou(周强)
Chin. Phys. B, 2023, 32 (**6**): 067801. DOI: 10.1088/1674-1056/acc0f5

Quantitative evaluation of LAL productivity of colloidal nanomaterials: Which laser pulse width is more productive, ergonomic, and economic?

Alena Nastulyavichus, Nikita Smirnov, and Sergey Kudryashov
Chin. Phys. B, 2022, 31 (**7**): 077803. DOI: 10.1088/1674-1056/ac5602

Dynamically controlled asymmetric transmission of linearly polarized waves in VO_2-integrated Dirac semimetal metamaterials

Man Xu(许曼), Xiaona Yin(殷晓娜), Jingjing Huang(黄晶晶), Meng Liu(刘蒙), Huiyun Zhang(张会云), and Yuping Zhang(张玉萍)
Chin. Phys. B, 2022, 31 (**6**): 067802. DOI: 10.1088/1674-1056/ac4bd3

Photonic Dirac cone and topological transition in a moving dielectric slab

Xinyang Pan(潘昕阳)[1], Haitao Li(李海涛)[1], Weijie Dong(董为杰)[1], Xiaoxi Zhou(周萧溪)[2], Gang Wang(王钢)[1,†], and Bo Hou(侯波)[3,‡]

[1] *School of Physical Science and Technology & Collaborative Innovation Center of Suzhou Nano Science and Technology, Soochow University, Suzhou* 215006, *China*

[2] *School of Optical and Electronic Information, Suzhou City University, Suzhou* 215104, *China*

[3] *Wave Functional Metamaterial Research Facility, The Hong Kong University of Science and Technology (Guangzhou), Guangzhou* 511400, *China*

(Received 13 May 2023; revised manuscript received 13 June 2023; accepted manuscript online 27 June 2023)

The moving media theory is applied to a photonic confined structure which is a continuous dielectric slab waveguide with the uniaxial anisotropy and without the discrete translational symmetry. The moving effect not only brings about non-reciprocity to the whole photonic band structure in the co-moving and counter-moving directions, but also leads to the topological transition of local degenerate points within the band diagram. We demonstrate through calculation that the type-II Dirac point can be turned into type-I Dirac point when the uniaxial slab is moving over certain speed. Our results provide a new approach to regulate the topology of degeneracy for two-dimensional photonic bands in the continuous translational symmetry condition.

Keywords: Dirac point, transition, moving, guided mode

PACS: 81.05.Xj, 67.10.Ba, 03.65.Pm, 78.67.Pt **DOI:** 10.1088/1674-1056/ace1d7

1. Introduction

The nodal degeneracies, such as Dirac points (DPs) and Weyl points (WPs), in band structures in various lattice systems may provide a platform to conduct the synergy investigation between the different fields of physics.[1–12] For instance, the structural transition between type-I and type-II Dirac points is considered in condensed matter physics and is proposed to explore the black hole physics and astrophysics.[13–17] Therefore, the design of nodal degeneracies and the study of their transitions in momentum space are of fundamental interest. Through dispersion engineering, the two-dimensional (2D) DPs can be realized with photonic guided modes along the direction where continuous translational symmetry retains.[18–20] Straightforwardly, a two-band degeneracy can be designed between the transverse electric (TE) and transverse magnetic (TM) guided modes for a slab of dielectric medium, and a simple approach is to introduce the in-plane anisotropy to cause the band crossing between TE and TM branches with mirror symmetry protection.[21] Furthermore, because of the simultaneous positivity of the slopes of both guided modes, the resultant degeneracy is essentially of type-II cone in the continuous medium case, as illustrated in Fig. 1(a). To evoke the type-I cone and the transition between both cones, Bloch periodicity is employed to reverse the slope of the band, where the dispersion of the guided modes is back-folded within the first Brillouin zone arising from spatial periodicity in Bloch lattices.[18,22] Notably, the graphene lattice is an excellent 2D platform to engineer the type-I Dirac cone. Even remarkably, double Dirac cone (type-I) can be realized with photonic periodical structures through aligning TM-polarized cone and TE-polarized cone at the same frequency.[23,24] However, how to obtain the type-I cone in the uniform medium lack of the discrete translational symmetry is a question.

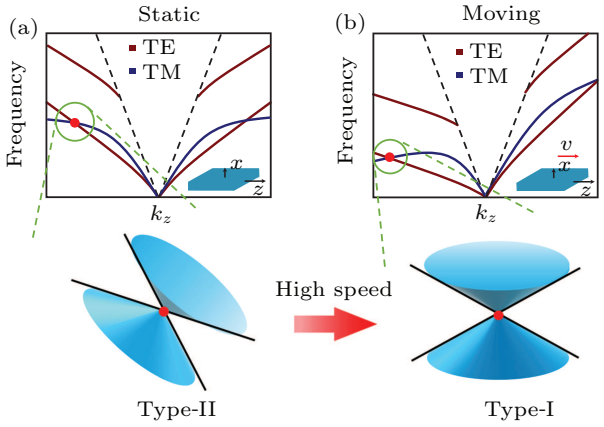


Fig. 1. Sketches of guided modes (upper row) and zoomed Dirac cones (lower row) around the degenerate point in a uniaxial crystal slab waveguide with in-plane optical axis for (a) static case and (b) moving case, respectively. The slab with the finite thickness along the x direction is illustrated by the insets. The moving direction is assumed along the optical axis, *i.e.*, horizontal direction, labeled as z axis in the insets. The dark red lines represent TE modes and the dark blue lines represent TM modes, and the dash line denotes the light line in air.

†Corresponding author. E-mail: phwanggang@gmail.com

‡Corresponding author. E-mail: bohou@hkust-gz.edu.cn

© 2023 Chinese Physical Society and IOP Publishing Ltd

Here, we propose a method to realize the 2D type-I DPs in the uniform dielectric medium slab. This method dates to the 19th century when Fresnel predicted the dragging of light in moving media.[25] The Fresnel's theory was verified by Fizeau's celebrated experiment with flowing water, exposing the difference of the speed of light in the up-stream and down-stream direction.[26] In the study, we find that moving the dielectric slab can lift the otherwise overtilted Dirac cone along the counter-moving direction, because the dragging effect manifests very different intensity to TE and TM guided modes. Therefore, we may realize the transition of the Dirac cone from type-II to type-I in the continuous medium through tunning the moving speed of the slab, as shown in Fig. 1(b).

2. Electromagnetic parameters of moving uniaxial crystal slabs

In the following, we will discuss the dispersion relations in an inertial frame S fixed to the laboratory where a uniaxial medium is moving. We attach an inertial frame S′ to the medium (choosing the optical axis as one of coordinate axes, e.g., z' axis) where the medium is observed being rest and has the uniaxial permittivity tensor diag $[\varepsilon', \varepsilon', \varepsilon_z']$ and the uniaxial permeability tensor diag $[\mu', \mu', \mu_z']$ (the isotropic permittivity or permeability case can be obtained through making $\varepsilon' = \varepsilon_z'$ or $\mu' = \mu_z'$). Consider the simple case in which the coordinate axes of S and S′ are parallel to each other, that is, orthonormal vectors $\hat{x} \| \hat{x}'$, $\hat{y} \| \hat{y}'$, and $\hat{z} \| \hat{z}'$. The medium, *i.e.*, the frame S′, is moving with velocity $\bar{v}$ in the frame S. The Lorentz transformation of the electromagnetic field can be written as[27]

$$\begin{bmatrix} c\bar{D}' \\ \bar{H}' \end{bmatrix} = \gamma \begin{bmatrix} \overline{\overline{\alpha}}^{-1} & \overline{\overline{\beta}} \\ -\overline{\overline{\beta}} & \overline{\overline{\alpha}}^{-1} \end{bmatrix} \cdot \begin{bmatrix} c\bar{D} \\ \bar{H} \end{bmatrix}, \tag{1}$$

$$\begin{bmatrix} \bar{E}' \\ c\bar{B}' \end{bmatrix} = \gamma \begin{bmatrix} \overline{\overline{\alpha}}^{-1} & \overline{\overline{\beta}} \\ -\overline{\overline{\beta}} & \overline{\overline{\alpha}}^{-1} \end{bmatrix} \cdot \begin{bmatrix} \bar{E} \\ c\bar{B} \end{bmatrix}, \tag{2}$$

where c is the speed of light in vacuum and

$$\bar{\beta} = \beta_x \hat{x} + \beta_y \hat{y} + \beta_z \hat{z} = \frac{\bar{v}}{c}, \tag{3}$$

$$\gamma = \frac{1}{\sqrt{1-\beta^2}} = \frac{1}{\sqrt{1-(\beta_x^2+\beta_y^2+\beta_z^2)}}, \tag{4}$$

$$\overline{\overline{\alpha}} = \overline{\overline{I}} + (\gamma-1)\frac{\bar{\beta}\bar{\beta}}{\beta^2} = \begin{bmatrix} 1 & 0 & 0 \\ 0 & 1 & 0 \\ 0 & 0 & 1 \end{bmatrix} + \frac{\gamma-1}{\beta^2} \begin{bmatrix} \beta_x^2 & \beta_x\beta_y & \beta_x\beta_z \\ \beta_y\beta_x & \beta_y^2 & \beta_y\beta_z \\ \beta_z\beta_x & \beta_z\beta_y & \beta_z^2 \end{bmatrix}, \tag{5}$$

$$\overline{\overline{\beta}} = \begin{bmatrix} 0 & -\beta_z & \beta_y \\ \beta_z & 0 & -\beta_x \\ -\beta_y & \beta_x & 0 \end{bmatrix}. \tag{6}$$

From Eqs. (1) and (2) we can obtain the constitutive matrix of the moving medium in the frame S:

$$\overline{\overline{C}} = \begin{bmatrix} \varepsilon & 0 & 0 & 0 & \xi & 0 \\ 0 & \varepsilon & 0 & -\xi & 0 & 0 \\ 0 & 0 & \varepsilon_z & 0 & 0 & 0 \\ 0 & -\xi & 0 & \mu & 0 & 0 \\ \xi & 0 & 0 & 0 & \mu & 0 \\ 0 & 0 & 0 & 0 & 0 & \mu_z \end{bmatrix} = \begin{bmatrix} \overline{\overline{\varepsilon}} & \overline{\overline{\xi}} \\ -\overline{\overline{\xi}} & \overline{\overline{\mu}} \end{bmatrix}, \tag{7}$$

in which we have assumed that the medium moves along the optical axis or the z direction, namely, $\beta_x = 0$, $\beta_y = 0$, and $\bar{\beta} = \beta\hat{z}$. And we have

$$\varepsilon = \frac{\varepsilon'(1-\beta^2)}{(1-n'^2\beta^2)}, \quad \varepsilon_z = \varepsilon_z', \tag{8}$$

$$\mu = \frac{\mu'(1-\beta^2)}{(1-n'^2\beta^2)}, \quad \mu_z = \mu_z', \tag{9}$$

$$\xi = \frac{-\beta\left(n'^2-1\right)}{c\left(1-n'^2\beta^2\right)}, \tag{10}$$

$$n'^2 = c^2\mu'\varepsilon', \tag{11}$$

where $\overline{\overline{\xi}}$ is the magnetoelectric coupling matrix caused by motion. Therefore, the static uniaxial medium can become a bi-anisotropic medium in the frame S when it is moving. Furthermore, the permittivity component ε and the permeability component μ that are orthogonal to the z direction are related to normalized velocity β, and so we can adjust the moving speed of the medium to achieve the purpose of regulating the electromagnetic parameters.

The bulk modes of EM wave in moving media have been investigated intensely.[27] For the ordinary wave, E-field has zero component along the propagating direction $\hat{k} = \bar{k}/k$ and nonzero components being transverse to the propagating direction. The dispersion relation can be obtained as follows:

$$\varepsilon\omega^2 = \frac{k_\perp^2}{\mu_z} + \frac{(k_\parallel - \xi\omega)^2}{\mu}, \tag{12a}$$

where $k_\parallel$ ($k_\perp$) represents the wave number parallel (orthogonal) to the moving direction of the medium and satisfies $k_\parallel^2 + k_\perp^2 = k^2$. For the extraordinary wave, E-field has nonzero component being both parallel to $\hat{k}$ and transverse to $\hat{k}$. The dispersion relation is

$$\mu\omega^2 = \frac{k_\perp^2}{\varepsilon_z} + \frac{(k_\parallel - \xi\omega)^2}{\varepsilon}. \tag{12b}$$

The dispersion of the ordinary wave is plotted in Fig. 2, which shows the Fresnel drag by the moving medium. When the medium is at rest ($\beta = 0$), the dispersion curve is displayed as a circle, where the nonmagnetic condition $\mu_z' = \mu' = \mu_0$ has been applied. In the velocity range where $1 - n'^2\beta^2 > 0$, the curve is stretch into an ellipse which is symmetric about

the $k_{\parallel}$ axis, we call it non-relativistic zone. For the velocities where $1-n'^2\beta^2<0$, the ellipse is transformed into a hyperbola. This is the relativistic case and the velocity region is called the Cerenkov zone. The velocity that divides the non-relativistic zone and the Cerenkov zone is $\beta = 1/n'$, which is the speed of light that propagates in the stationary medium. In addition, the reversed transition of the iso-frequency contour from hyperbola to ellipse may be realized when assuming the hyperbolic property for the medium in the frame S′,[28–32] seeing the supplementary material (Section A).

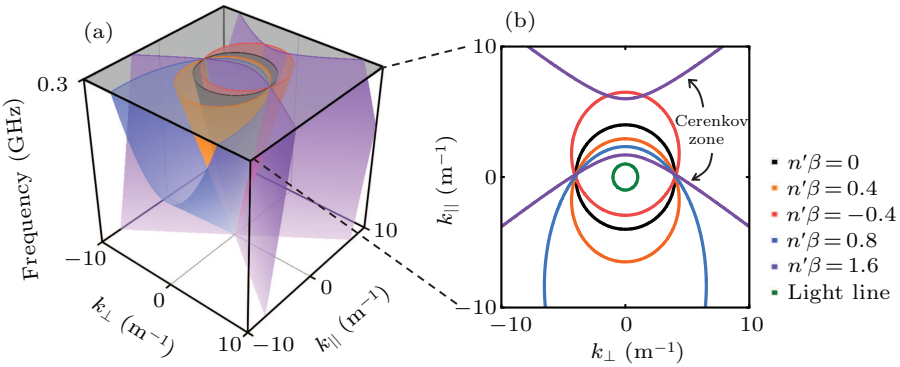


Fig. 2. (a) Bulk dispersion of the ordinary wave at different velocities with $n' = 4$. (b) The iso-frequency contour in the bulk medium at $\omega = 0.3$ GHz with different velocities labeled, respectively, by different colors. The green line represents the light cone in air at $\omega = 0.3$ GHz. The Cerenkov zone is pointed out with an arrow. The results of the extraordinary wave are similar, except the uniaxial anisotropy indicated by $\varepsilon'_z \neq \varepsilon'$, and are not plotted here.

3. Guided modes in the moving uniaxial crystal slab

Equation (12) is the dispersion relation of EM wave in the bulk moving material, and in contrast the investigated slab has a finite thickness d, as shown in Fig. 3(a). To solve the guided modes in the moving slab, we impose the boundary condition that requires both tangential electric field and magnetic field are continuous on the boundary.[27] In the first place, we consider the guided modes with the propagating direction along the optical axis, and the mirror symmetry $M_y : (x,y,z) \to (x,-y,z)$ enables both TE and TM modes. Thus, we can obtain the characteristic equation for TE modes in the moving dielectric slab waveguide in the frame S:

$$\frac{2\alpha}{\mu_{zr}} k_x \cos k_x d + \left(\alpha^2 - \frac{k_x^2}{\mu_{zr}^2}\right) \sin k_x d = 0, \tag{13}$$

in which $\mu_{zr} = \mu_z/\mu_0$ and k_x satisfies Eq. (12a) in the region I, seeing Fig. 3(a). Likewise, we have the characteristic equation for TM mode:

$$\left(\alpha^2 - \frac{k_x^2}{\varepsilon_{zr}^2}\right) \sin k_x d + \frac{2\alpha k_x}{\varepsilon_{zr}} \cos k_x d = 0, \tag{14}$$

in which $\varepsilon_{zr} = \varepsilon_z/\varepsilon_0$ and k_x satisfies Eq. (12b) in the region I. In the above, α is the evanescent wavenumber in regions II and III, satisfying $k_z^2 - \alpha^2 = \omega^2\mu_0\varepsilon_0$.

For concreteness, the parameters of the stationary medium are chosen as $d = 2$ mm, $\varepsilon' = 16\varepsilon_0 = (n'_{\rm o})^2$, $\varepsilon'_z = 100\varepsilon_0 = (n'_{\rm e})^2$, and $\mu' = \mu'_z = \mu_0$, so that $n' = n'_{\rm o} = 4$. It is has known that the nonmagnetic planar slabs have been extensively used as basic waveguides in microwave engineering and devices where a broad horizon of dielectric materials, e.g., high-k printed circuit board (PCB) and ceramics, is

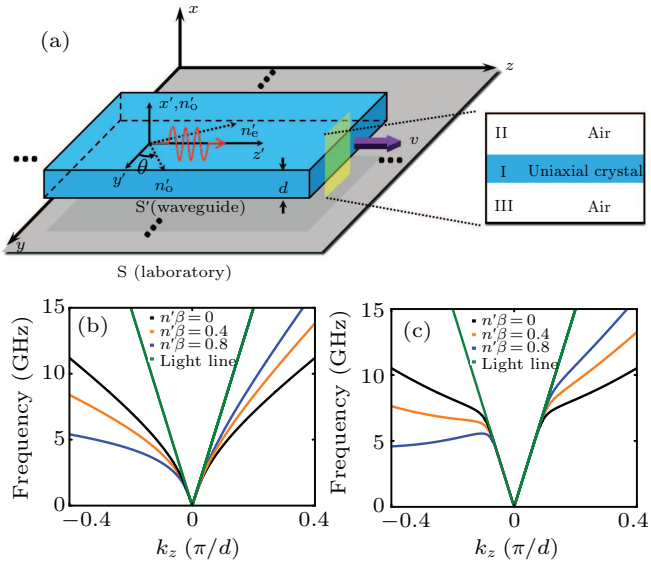


Fig. 3. (a) The schematic picture of the uniaxial crystal slab waveguide, where (x,y,z) denotes the reference frame S, (x',y',z') denotes the reference frame S′, and $(n'_{\rm o}, n'_{\rm o}, n'_{\rm e})$ is the dielectric principal axes for the uniaxial anisotropy. The red arrow represents the propagation direction of electromagnetic wave. The purple arrow shows the velocity of the slab relative to the frame S. The angle θ denotes the in-plane rotation of the optical axis and the velocity direction. The panel in the right shows the three layers structure in our system. (b) and (c) Dispersion diagram of the lowest band of TE and TM mode when $\theta = 0$, where the black, orange, and blue lines correspond to the velocities $n'\beta = 0$, $n'\beta = 0.1$, and $n'\beta = 0.2$, respectively, and green line represents the light line.

available.[33,34] The dispersion curves of the lowest band of TE and TM modes for different velocity are depicted in Figs. 3(b) and 3(c). We limit the normalized wavenumber $k_z/(\pi/d)$ from -0.4 to 0.4 and calculate the characteristic equation in non-relativistic case. When the waveguide stays stationary in the frame S ($\beta = 0$), the dispersion relation of ωk_z consists of two branches which are symmetric about the ω-axis (black line in Figs. 3(b) and 3(c)), in agreement with the parity symmetry

in the stationary system. The two branches correspond to the waves traveling in opposite directions, respectively. Furthermore, the slope of TE and TM modes are both positive (negative) in $+z$ direction ($-z$ direction). However, the parity symmetry is broken as soon as the medium begin to move, which causes the $+z$ and $-z$ directions inequivalent. Then, as we increase the velocity, the asymmetry of the dispersion is more evident. What is more, comparing $\beta = 0.1$ (that is, $n'\beta = 0.4$) with the case of $\beta = 0.2$ (that is, $n'\beta = 0.8$), the sign of group velocity ($\mathrm{d}\omega/\mathrm{d}k$) of TM mode has a switch along the negative k_z-direction and the switching point is at $k_z \approx -0.104(\pi/d)$, whereas the group velocity of TE mode keeps the sign unchanged in the range from $k_z = 0$ to $k_z = -0.4(\pi/d)$. In terms of the classification of DPs, where the type-I DP comes from the crossing of two bands with opposite slope, the normalized velocity β of the medium should not be lower than 0.1 to obtain the crossing between TE and TM bands with opposite slope. To display an explicit result, we take the velocity $\beta = 0$ and $\beta = 0.16$ in the following calculation.

4. Type-I Dirac degeneracy in the moving uniaxial crystal slab

As shown in Figs. 4(a) and 4(b), the analytical results are solved using Eqs. (13) and (14). When $\beta = 0$, the TE_2 (subscript labeling the TE band number) band crosses linearly with the TM_3 (subscript labeling the TM band number) band at point A$'$ at the frequency 23.7 GHz, see Fig. 4(a), where their slope is of the same sign. In contrast, when $\beta = 0.16$, the degeneracy labeled as point A is reduced to 18.36 GHz due to the moving effect, see Fig. 4(b), where their slope is noticed of opposite sign. The analytical results can be verified by numerical calculations. Using the eigenmode solver of finite-element simulation software COMSOL and representing the moving effect with bi-anisotropic parameters, we calculate the dispersion of the stationary and moving uniaxial crystal slab for TE and TM modes at $\beta = 0$ and $\beta = 0.16$, and plot them in Figs. 4(a) and 4(b). It is seen that good agreement between analytical and numerical results is achieved. In addition, either TE or TM mode can be further classified with even or odd parity, because of the mirror symmetry M_x (the system having the mirror plane $x = d/2$). The parity is alternative for either TM or TE modes. Namely, TM_n modes with even mode number n and TE_n modes with odd mode number n are antisymmetric, and TM_n modes with odd n and TE_n modes with even n are symmetric. The numerical calculation reveals that TE_2 and TM_3 have the same parity, and the insets in Figs. 4(a) and 4(b) are the H_z map of TE_2 mode from COMSOL.

In order to exhibit the complete dispersion structure around the degenerate points A$'$ and A, we need calculate the band diagram $\omega(k_y, k_z)$. In the calculation, we first rotate the in-plane dielectric principal axes around the x direction by an angle θ, as shown in Fig. 3(a). The non-diagonalized permittivity (permeability) tensor $\overline{\overline{\varepsilon}}_\theta$ ($\overline{\overline{\mu}}_\theta$) after rotation can be written in the frame S as

$$\overline{\overline{\varepsilon}}_\theta = \begin{bmatrix} \varepsilon_{xx} & 0 & 0 \\ 0 & \varepsilon_{yy} & \varepsilon_{yz} \\ 0 & \varepsilon_{zy} & \varepsilon_{zz} \end{bmatrix}, \tag{15}$$

$$\overline{\overline{\mu}}_\theta = \begin{bmatrix} \mu_{xx} & 0 & 0 \\ 0 & \mu_{yy} & \mu_{yz} \\ 0 & \mu_{zy} & \mu_{zz} \end{bmatrix}, \tag{16}$$

in which

$$\varepsilon_{xx} = \varepsilon, \quad \mu_{xx} = \mu, \tag{17}$$

$$\varepsilon_{yy} = \varepsilon\cos^2\theta + \varepsilon_z \sin^2\theta,$$

$$\mu_{yy} = \mu\cos^2\theta + \mu_z \sin^2\theta, \tag{18}$$

$$\varepsilon_{zz} = \varepsilon_z\cos^2\theta + \varepsilon \sin^2\theta,$$

$$\mu_{zz} = \mu_z\cos^2\theta + \mu \sin^2\theta, \tag{19}$$

$$\varepsilon_{yz} = \varepsilon_{zy} = (\varepsilon - \varepsilon_z)\sin\theta\cdot\cos\theta,$$

$$\mu_{yz} = \mu_{zy} = (\mu - \mu_z)\sin\theta\cdot\cos\theta. \tag{20}$$

And the magnetoelectric coupling matrix $\overline{\overline{\xi}}_\theta$ after rotation has the form in the frame S:

$$\overline{\overline{\xi}}_\theta = \begin{bmatrix} 0 & \xi\cos\theta & \xi\sin\theta \\ -\xi\cos\theta & 0 & 0 \\ -\xi\sin\theta & 0 & 0 \end{bmatrix}. \tag{21}$$

The θ-dependence of EM parameters is derived in the supplementary material (Section B). Then, we assume that the wave still propagate along the z direction and express the electric fields and magnetic fields in different regions. Because the mirror symmetry $\mathcal{M}_y$ is broken due to the rotation, the guided modes are no longer pure TE or TM mode but are their combination which we call hybrid mode. The characteristic equation for hybrid mode is solved by matching boundary conditions, which gives us the dispersion $\omega_\theta(k_z)$. The calculated results are plotted in the right panels of Figs. 4(a) and 4(b), and three θ-cut dispersions for the $\beta = 0.16$ case are shown in Figs. 5(a)–5(c). When the medium is in motion, we can see from Figs. 5(a)–5(c) that the degeneracy of point A is lifted upon θ being nonzero. So is the static case, too. This is because the $\mathcal{M}_y$ symmetry does not exist anymore and meanwhile two degenerate bands have the same parity under $\mathcal{M}_x$.[21]

In the static case, TE_2 and TM_3 linearly cross at the degenerate point A$'$ and form an over-tilted Dirac cone, which gives rise to a type-II DP in momentum space, as shown in the right panel of Fig. 4(a). In the moving case of $\beta = 0.16$, both modes cross with positive and negative group velocities and display a type-I cone or DP, as illustrated in the right panel of Fig. 4(b). Furthermore, the tilting term in the type-I DP Hamiltonian can be entirely neglected, seeing the supplementary Material (Section C), which demonstrates an upright conical band structure near the degenerate point. Therefore, by employing the motion of medium we can "drag" the Dirac point from type-II to type-I.

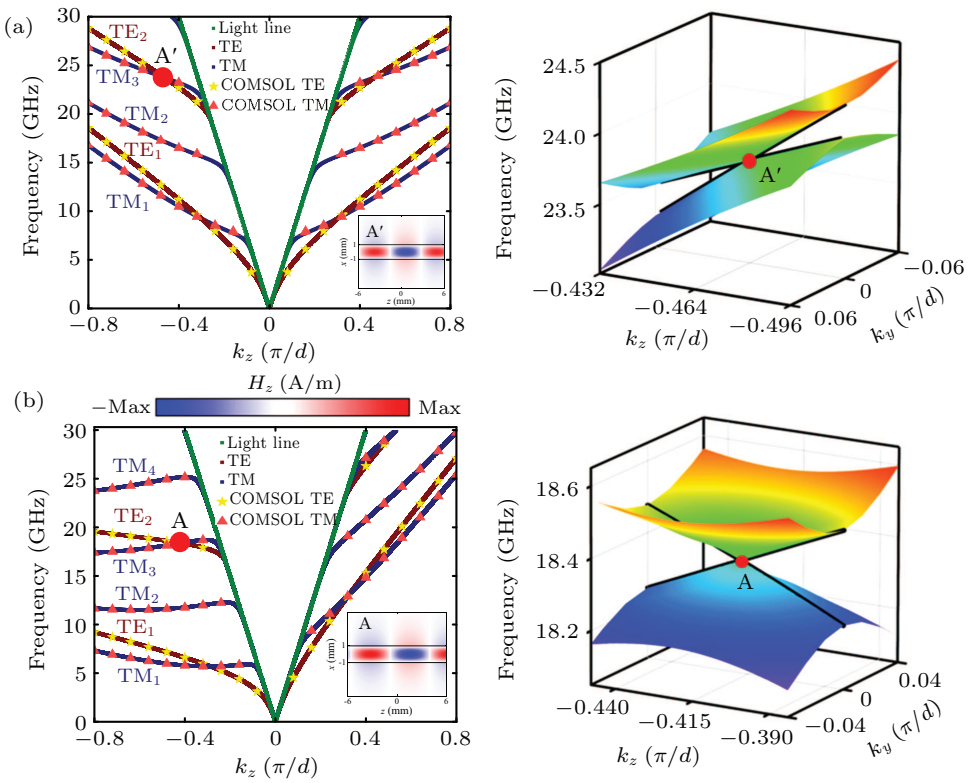


Fig. 4. (a) The dispersion diagram of TE modes and TM modes when $\theta = 0°$ in the static slab. (b) The dispersion diagram of TE modes and TM modes when $\theta = 0°$ in the moving slab with $\beta = 0.16$. The left illustrations in panels (a) and (b) show the analytical and numerical results, where the former is represented by the solid lines and the latter by the solid symbols. The degenerate points (red points) are marked with A and A′. The H_z maps of TE modes at the two degenerate points are displayed as insets. The right illustrations in panels (a) and (b) show the band structure around the degenerate point, and the linear dispersion in k_z-direction is marked by black lines.

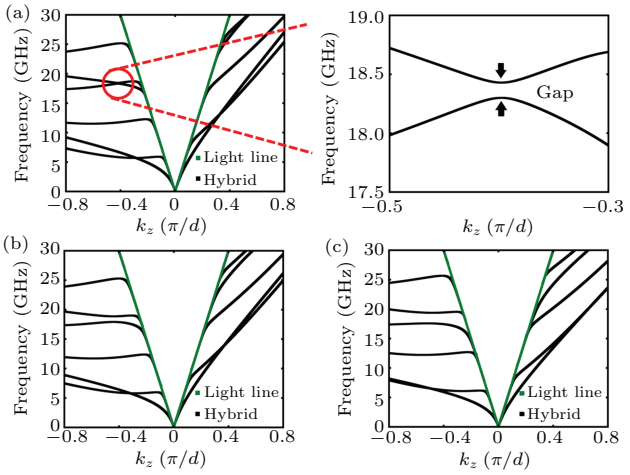


Fig. 5. The dispersion $\omega_\theta(k_z)$ of hybrid modes in the moving slab when (a) $\theta = 2°$, (b) $\theta = 15°$, and (c) $\theta = 30°$.

5. Discussion

It is also noted in Fig. 4 that a lower-frequency degeneracy is caused by the crossing between the fundamental TE and TM modes (TE_1 and TM_1). The calculation reveals that the degeneracy transforms topologically from type-II to type-I upon moving, see Figs. 4(a) and 4(b), and furthermore the degeneracy is not lifted in three θ-cut plots though its frequency and the momentum are shifting, see Figs. 5(a)–5(c). In fact, it is a line degeneracy protected by the symmetry $\mathcal{M}_x$ (TE_1 and TM_1 having the opposite parity under $\mathcal{M}_x$). The line degeneracy is the type-II Dirac line in the static case,[21] and its tilting will be regulated in a θ-dependent way by the velocity in the moving case.

On the other hand, the spatial inversion symmetry in our system is broken due to the moving, and $\omega(k_z)$ is not symmetrical along $+k_z$ and $-k_z$ directions, and our study is mainly focused on the $-k_z$ direction. As an accompanying effect, the type-II degeneracies in the $+k_z$ direction become even more titled when the slab changes from the static state to the moving state, which is the consequence of the spatial inversion symmetry broken by the moving.

Last, we make a discussion from an experimental point of view. Although achieving a speed of $0.16c$ is challenging, a moving medium can be effectively simulated by using space–time-modulated methodology.[35] Therefore, by changing the electromagnetic parameters of a static and anisotropic medium in both temporal and spatial domains, the similar effects to the band structure as those in our study would be anticipated both theoretically and experimentally.

6. Conclusion

In conclusion, the physics of Fizeau's flowing water experiment has been applied to a photonic confined structure which is a continuous dielectric slab waveguide and where the uniaxial anisotropy is involved. The moving effect not only

brings about non-reciprocity to the band structure in the up-stream and down-stream directions, but also leads to the topological transition of local degenerate points within the band structure. We calculated an explicit case in which the type-II DP can be turned into type-I DP when the slab waveguide is moving. Our results provide a new approach to regulate the topology of degeneracy for 2D photonic bands in the continuous translational symmetry situation.

Acknowledgements

Project supported by the National Natural Science Foundation of China (Grant No. 12074279), the Major Program of Natural Science Research of Jiangsu Higher Education Institutions (Grant No. 18KJA140003), and the Priority Academic Program Development (PAPD) of Jiangsu Higher Education Institutions.

References

[1] Neto C A H, Guinea F, Peres N M R, Novoselov K S and Geim A K 2009 *Rev. Mod. Phys.* **81** 109
[2] Ozawa T, Price H M, Amo A, Goldman N, Hafezi M, Lu L, Rechtsman M C, Schuster D, Simon J, Zilberberg O and Carusotto I 2019 *Rev. Mod. Phys.* **91** 015006
[3] Armitage N P, Mele E J and Vishwanath A 2018 *Rev. Mod. Phys.* **90** 015001
[4] Lu L, Wang Z Y, Ye D X, Ran L X, Fu L, Joannopoulos J D and Soljacic M 2015 *Science* **349** 622
[5] Gao W, Yang W, Lawrence W, Fang W, Béril B and Zhang S 2016 *Nat. Commun.* **7** 12435
[6] Yang B, Guo Q, Tremain B, Barr L E, Gao W, Liu H, Béril B, Xiang Y, Fan D, Hibbins A P and Zhang S 2017 *Nat. Commun.* **8** 97
[7] Yang B, Guo Q, Tremain B, Liu R, Barr L E, Yan Q, Gao W, Liu H, Xiang Y, Chen J, Fang C, Hibbins A, Lu L and Zhang S 2018 *Science* **359** 1013
[8] Luo L, Deng W, Yang Y, Yan M, Lu J, Huang X and Liu Z 2022 *Phys. Rev. B* **106** 134108
[9] Liu G G, Zhou P, Yang Y, Xue H, Ren X, Lin X, Sun H X, Bi L, Chong Y and Zhang B 2020 *Nat. Commun.* **11** 1873
[10] Qiu P, Qiu W, Lin Z, Chen H, Ren J, Wang J X, Kan Q and Pan J Q 2017 *J. Phys. D: Appl. Phys.* **50** 335101
[11] Xiao M, Lin Q and Fan S 2016 *Phys. Rev. Lett.* **117** 057401
[12] Yang Y, Gao Z, Feng X, Huang Y X, Zhou P, Yang S A, Chong Y and Zhang B 2020 *Phys. Rev. Lett.* **125** 143001
[13] Volovik G E 2018 *Phys.-Usp.* **61** 89
[14] Westström A and Ojanen T 2017 *Phys. Rev. X* **7** 041026
[15] Guan S, Yu Z M, Liu Y, Liu G B, Dong L, Lu Y, Yao Y and Yang S A 2017 *npj Quantum Mater.* **2** 23
[16] Liu H, Sun J T, Song C, Huang H, Liu F and Meng S 2020 *Chin. Phys. Lett.* **37** 067101
[17] Jia H, Zhang R Y, Gao W, Zhang S and Chan C T 2021 *Phys. Rev. B* **104** 045132
[18] Joannopoulos J D, Meade R D, Johnson S G and Joshua N 2011 *Photonic Crystals: Molding the Flow of Light*, 2nd edn. (Princeton: Princeton University Press) pp. 27, 32
[19] Deng W M, Chen Z M, Li M Y, Guo C H, Tian Z T, Sun K X, Chen X D, Chen W J and Dong J W 2022 *Light Sci. Appl.* **11** 134
[20] Hu M, Zhang Y, Jiang X, Qiao T, Wang Q, Zhu S, Xiao M and Liu H 2021 *Light Sci. Appl.* **10** 170
[21] Pan X, Li H, Dong W, Zhou X, Xing K A, Hu C, Wang G and Hou B 2023 *Front. Phys.* **10** 1095669
[22] Fan S and Joannopoulos J D 2002 *Phys. Rev. B* **65** 235112
[23] Khanikaev A B, Mousavi S H, Tse W K, Kargarian M, MacDonald A H and Shvets G 2013 *Nat. Mater.* **12** 233
[24] He X T, Liu J W, Shi F L, Shen K, Chen W J, Chen X D and Dong J W 2022 *Sci. China- Phys. Mech. Astron.* **65** 284212
[25] Fresnel A J 1868 *Theory of light. Fifth section: various questions of optics*, letter to Arago, September 1818. In Oeuvers completes d'Augustin Fresnel, Vol. **2** 627
[26] Fizeau A H L 1851 *CR Hebd. Acad. Sci.* **33** 349
[27] Kong J A 2000 *Electromagnetic Wave Theory* (Cambridge: EMW Publishing) p. 879
[28] Aigner A, Dawes J M, Maier S A and Ren H 2022 *Light. Sci. Appl.* **11** 9
[29] Jia G, Luo J, Wang H, Ma Q, Liu Q, Dai H and Asgari R 2022 *Nanoscale* **14** 17096
[30] Ferrari L, Wu C, Lepage D, Zhang X and Liu Z 2015 *Prog. Quantum Electron.* **40** 1
[31] Poddubny A, Iorsh I, Belov P and Kivshar Y 2013 *Nat. Photon.* **7** 948
[32] Lee D, So S, Hu G, Kim M, Badloe T, Cho H, Kim J, Kim H, Qiu C W and Rho J 2022 *eLight* **2** 1
[33] Pozer D M 1998 *Microwave Engineering*, 2nd edn. (New York: John Wiley & Sons) p. 705
[34] https://www.rogerspcb.com.cn/
[35] Huidobro P A, Galiffi E, Guenneau S, Craster R V and Pendry J B 2019 *Proc. Natl. Acad. Sci. USA* **116** 24943